Model-based aerodynamic-angle attitude control of an atmospheric entry capsule

Published in Proc. AIAA Atmospheric Flight Mechanics Conference, Minneapolis, 13 - 16 August 2012.

Model-based aerodynamic-angle attitude control of an atmospheric entry capsule

Enrico Canuto[1] and José A. Ospina[2]
Politecnico di Torino, Torino, 10129, Italy

and

Marcello Buonocore[3]
Thales Alenia Space, Torino, 10146, Italy

The paper describes the attitude control system of a low lift-to-drag biconic atmospheric entry capsule based on the Embedded Model Control methodology. The control structure derives from the development of the attitude dynamics and kinematics written in terms of aerodynamic angles, instead of Euler/quaternion kinematics. A detailed development of the simplified set of equations linking the torques generated by the reaction control system with the time evolution of the aerodynamic angles is provided. The simplified set of equations becomes the core of the control algorithm. The bank angle dynamics is shown to be fourth-order and forced by yaw and roll torques. A dynamic dispatching technique is proposed for converting fourth-order dynamics into a pair of second order systems. Nonlinear dynamic inversion and active disturbance rejection are employed to handle gyroscopic torques, parametric errors and to compensate for angular variation of translational velocity. A bank reversal logic is designed to reduce the effect of bank reversals on the translational motion. The performance of the attitude control algorithm has been tested on a high fidelity simulator and relevant results are presented.

Nomenclature

μ	=	aerodynamic bank angle
α	=	total angle of attack
η	=	aerodynamic roll
ω_{l-m-n}	=	angular rate components in the body frame
$M_{T,l-m-n}$	=	components of the attitude command torque in the body frame
μ_{geo}	=	geometric bank angle
α_{geo}	=	angle of attack
β_{geo}	=	sideslip
$\vec{\omega}$	=	angular velocity vector
u_{l-m-n}	=	components of the angular acceleration in the body frame
$M_{a,l-m-n}$	=	components of the aerodynamic torque in the body frame
x_a	=	center-of-mass displacement along the body x axis (symmetry axis)
y_a	=	center-of-mass displacement along the body y axis

[1] Professor, Dipartimento di Automatica e Informatica, Corso Duca degli Abruzzi 24, 10129 Torino, Italy, enrico.canuto@polito.it, Senior Member.
[2] Research fellow, Dipartimento di Automatica e Informatica, Corso Duca degli Abruzzi 24, 10129 Torino, Italy, jose.ospina@polito.it. Now with Deimos Space, Ronda de Poniente 19, 28760 Tres Cantos, Madrid, Spain.
[3] GNC engineer, Business Segment Optical Observation and Science, Strada Antica di Collegno 253, 10146 Torino, Italy, marcello.buonocore@thalesaleniaspace.com.

c_A = axial aerodynamic coefficient
c_N = normal aerodynamic coefficient
$c_{l-m-n,a}$ = aerodynamic torque coefficients in the aerodynamic frame
$c_{l-m-n,CoM}$ = aerodynamic torque coefficients in the body frame
L = equivalent length from the aerodynamic data base
S = equivalent surface from the aerodynamic data base

I. Introduction

Guided entry is concerned with trajectory guidance and control of a vehicle entering the atmosphere either on the Earth or on other atmospheric planets such as Mars. The aerodynamic properties of the vehicle are arranged in such a way to cause the entry lift vector, whether adequately oriented, to control and adjust the vehicle trajectory. As such, an attitude control system which is capable of a fast and accurate orientation of the lift vector, becomes the actuator of the vehicle entry path. Guided entry has been identified by Wolf [1] as a necessary technology for the reduction of the landing site dispersion on Mars from the 80-200 km of the previous missions to below 10 km as in the on-going US Mars Science Laboratory, and in the limit to achieve pin-point landing as envisaged by future missions.

The guided entry algorithms developed by the authors are subdivided into path planning, reference path tracking and attitude control. This paper is devoted to the attitude control; path-planning and reference path-tracking algorithms are detailed in Canuto et al. [2].

As a key point, attitude control abandons Euler-angle and quaternion kinematics in favor of the more complex aerodynamic angles. Kinematics is derived by differentiating the whole sequence of angles that rotate the local-vertical–local-horizontal frame into body axes. Three aerodynamic angles, namely, bank angle, total angle-of-attack and (aerodynamic) roll, constitute the sequence converting local trajectory axes (aligned with the vehicle path) to the body frame. As the vehicle attitude must be faster actuated than the vehicle direction of motion, aerodynamic angles dominate kinematic equations, making them to approach Euler kinematics. As an advantage of the formulation, aerodynamic angles are the degrees-of-freedom of the aerodynamic force (lift) capable of controlling the vehicle entry path. Specifically, restricting the treatment to a biconic capsule with a fixed center of mass (CoM), the total angle of attack α and the (aerodynamic) roll η shall fluctuate around their natural equilibriums. On the contrary, the bank angle must be adjusted by a reaction control system, to drive the flight-path angle γ and heading χ of the vehicle entry trajectory (see Canuto et al. [2] for the translation state equations).

Attitude control has been designed to satisfy the requirements:

1) The bank angle is the unique degree-of-freedom which is continuously adjusted to drive the 3D entry path longitudinal and lateral components along the reference path. The 2D longitudinal motion is driven by controlling the magnitude of the bank angle cosine. The lateral motion is controlled by toggling the sign of the bank angle sine at specific time instants giving rise to the so-called bank reversal maneuvers (BRM).
2) Total angle of attack and roll must be stabilized around their natural (unknown) equilibriums.

The resulting attitude control deviates from the literature both in the structure and in the algorithms. Brugarolas et al. [3] propose a proportional plus derivative controller with a dead-band, whereas Kron et. al. [4] propose non-linear dynamic inversion. Here the attitude algorithms exploit aerodynamic angles instead of the Euler and quaternion kinematics, and the algorithm structure and tuning follow the Embedded Model Control (EMC) guidelines (see Canuto et al. [5,6,7,8]). Model and control design prove that the total angle-of-attack can be decoupled from roll and bank-angle dynamics, and that the latter cannot be further decoupled. To cope with the fourth-order complexity of the bank-angle and roll dynamics, which is driven by yaw and roll torques, a dynamic dispatching technique - actuating yaw and roll torques - has been devised which is capable of forcing the bank angle to become the output of a second-order dynamics, and, at the same time, of preventing roll excitation.

The paper is organized as follows. First aerodynamic-angle kinematics is developed and simplified, obtaining an equation structure which is at the basis of the attitude control algorithm. The latter is subdivided into two components. Open loop is in charge of the bank angle reference. Closed-loop is capable of keeping the navigated bank angle around its reference trajectory and of stabilizing angle of attack and roll around their natural (unknown) equilibriums.

II. Aerodynamic-angle kinematics and dynamics

A. Definition of aerodynamic angles

Attitude kinematics of a rigid body can be formulated in several manners depending on the attitude definition, from Euler angles to quaternions, to rotation matrices. In this paper, the attitude is formulated in terms of aerodynamic angles, as they favor the design and implementation of an attitude control capable of modulating aerodynamic forces.

The frames of reference R_x, where x is a generic subscript, are defined with the aid of Fig 1. It shows the sequence of rotations around Cartesian axes (Euler angles) converting the inertial frame R_I into the body frame R_b. As Fig 1 shows, three main alternative sequences are possible.

1) The 'inertial-to-velocity' subsequence is common to the pair of sequences based on alternative aerodynamic angles. It passes through the planet-fixed frame R_M, the North-East-Down frame R_{NED} and the local-vertical-local-horizontal frame R_{LV}, ending into the velocity frame R_v. The angles are the planet rotation θ_M, the longitude λ and the latitude Λ, the heading angle χ and the flight path angle (FPA) γ.
2) The 'standard' aerodynamic subsequence starts from R_v, passes through the geometric wind frame $R_{w,geo}$ and the stability frame R_s, to end into the body frame R_b. The set includes the angle of attack α_{geo}, the sideslip β_{geo} and the geometrical bank angle μ_{geo}. The sequence is a Tayt-Brian 1-3-2 sequence.
3) The 'axis-symmetric' aerodynamic subsequence starts from R_v, passes through the wind frame R_w and the axis-symmetric frame R_{as}, ending into the body frame R_b. The set includes the total angle of attack α, the (aerodynamic) roll η and the bank angle μ. The sequence is a proper-Euler 1-2-1 sequence. The roll η corresponds to $-\Phi$ in Chapter 4 of Gallais [9].
4) The last sequence, rotating R_{NED} into R_b, can be usually selected to be either 3-2-1 $\{\psi,\theta,\varphi\}$ or 1-2-3 $\{\varphi,\theta,\psi\}$.

Of the two sets of aerodynamic angles, namely the standard set $\{\alpha_{geo},\beta_{geo},\mu_{geo}\}$ and the axis-symmetric $\{\alpha,\eta,\eta\}$, the latter is usually chosen when the aerodynamic shape of the body is axisymmetric, because, in that case, aerodynamic forces only depend on the total angle of attack. In general, one may select between alternative bank angles: the geometrical and the aerodynamic bank angles μ_{geo} and μ. Here the bank angle μ is selected (together with the axisymmetric set), because it simplifies the expression of the aerodynamic forces in the velocity frame R_v.

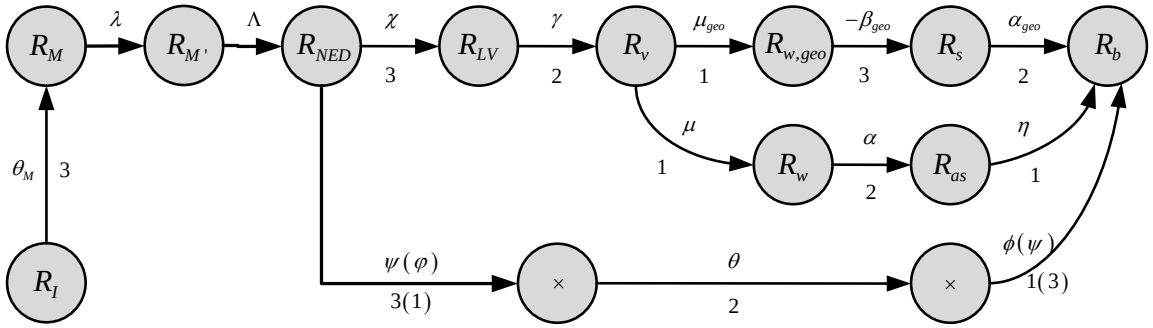

Fig 1. Alternative sequences of frames and relevant angular rotations.

B. Kinematics of aerodynamic angles

The time derivatives of the aerodynamic angles are obtained as a function of the angular rate components in the body frame, and of the time derivatives of the angular rotations from R_I to R_v in Fig 1. To this end, the angular rate vector $\vec{\omega}$ is written as the sum of the angular rate vector of each rotation, as follows

$$\vec{\omega}(t) = \dot{\theta}_M \vec{k}_I + \dot{\Lambda}\vec{k}_M + \dot{\lambda}\vec{j}\,''+ \dot{\chi}\,\vec{k}_{NED} + \dot{\gamma}\,\vec{j}_{LV} + \dot{\mu}\,\vec{i}_v + \dot{\alpha}\,\vec{j}_w + \dot{\eta}\vec{i}_{as}\,, \tag{1}$$

where $\vec{i}_x$, $\vec{j}_x$ and $\vec{k}_x$ are the first, second and third unit vector of a generic frame indicated by the subscript x. The components of (1) in R_b can be written as

$$\begin{bmatrix}\omega_l\\ \omega_m\\ \omega_n\end{bmatrix} = T_I^b\begin{bmatrix}0\\0\\1\end{bmatrix}\dot{\theta}_M + T_M^b\begin{bmatrix}0\\0\\1\end{bmatrix}\dot{\Lambda} + T_{M'}^b\begin{bmatrix}0\\1\\0\end{bmatrix}\dot{\lambda} + T_{NED}^b\begin{bmatrix}0\\0\\1\end{bmatrix}\dot{\chi} + T_{LV}^b\begin{bmatrix}0\\1\\0\end{bmatrix}\dot{\gamma} + T_v^b\begin{bmatrix}1\\0\\0\end{bmatrix}\dot{\mu} + T_w^b\begin{bmatrix}0\\1\\0\end{bmatrix}\dot{\alpha} + T_{as}^b\begin{bmatrix}1\\0\\0\end{bmatrix}\dot{\eta}\,, \tag{2}$$

where T_x^y is the transformation matrix from R_x to R_y. Solving (2) for $\dot{\eta}$, $\dot{\alpha}$ and $\dot{\mu}$, and simplifying trigonometric notations into $c_\theta = \cos\theta$, $s_\theta = \sin\theta$ and $t_\theta = \tan\theta$, where θ denotes a generic angle, yields the 'aerodynamic' kinematic equation

$$\begin{bmatrix}\dot{\eta}\\ \dot{\alpha}\\ \dot{\mu}\end{bmatrix} = \begin{bmatrix}1 & -\dfrac{s_\eta c_\alpha}{s_\alpha} & -\dfrac{c_\eta c_\alpha}{s_\alpha}\\ 0 & c_\eta & -s_\eta\\ 0 & \dfrac{s_\eta}{s_\alpha} & \dfrac{c_\eta}{s_\alpha}\end{bmatrix}\begin{bmatrix}\omega_l\\ \omega_m\\ \omega_n\end{bmatrix} + \begin{bmatrix}f_\eta\left(\dot{\theta}_M,\dot{\Lambda},\dot{\lambda},\dot{\chi},\dot{\gamma}\right)\\ f_\alpha\left(\dot{\theta}_M,\dot{\Lambda},\dot{\lambda},\dot{\chi},\dot{\gamma}\right)\\ f_\mu\left(\dot{\theta}_M,\dot{\Lambda},\dot{\lambda},\dot{\chi},\dot{\gamma}\right)\end{bmatrix}. \tag{3}$$

Equation (3) looks similar to Euler kinematics, except for the aerodynamic angles, and the 'parasitic' functions $f_\eta(\cdot)$, $f_\alpha(\cdot)$ and $f_\mu(\cdot)$. The latter ones express dependence of the aerodynamic angles on the time-varying local vertical direction. The parasitic functions can be expanded as

$$\begin{aligned} f_\eta\left(\dot{\theta}_M,\dot{\Lambda},\dot{\lambda},\dot{\chi},\dot{\gamma}\right) = -s_\alpha^{-1}&\left(c_\lambda s_\gamma s_\mu + \left(c_\lambda c_\chi s_\gamma - s_\lambda c_\gamma\right)c_\mu\right)\omega_M + \left(c_\lambda s_\chi s_\lambda + \left(c_\lambda c_\chi s_\gamma - s_\lambda c_\gamma\right)c_\mu\right)\dot{\Lambda}\\ &+\left(c_\chi s_\mu - s_\chi s_\gamma c_\mu\right)\dot{\lambda} - s_\mu\dot{\gamma} + c_\gamma c_\mu\dot{\chi}\end{aligned}, \tag{4}$$

$$\begin{aligned} f_\alpha\left(\dot{\theta}_M,\dot{\Lambda},\dot{\lambda},\dot{\chi},\dot{\gamma}\right) = &\left(\left(c_\lambda c_\chi s_\gamma - s_\lambda c_\gamma\right)s_\mu - c_\lambda s_\chi c_\mu\right)\omega_M + \left(\left(c_\lambda c_\chi s_\gamma - s_\lambda c_\gamma\right)s_\mu - c_\lambda s_\chi c_\mu\right)\dot{\lambda}\\ &+\left(-s_\chi s_\gamma s_\mu - c_\chi c_\mu\right)\dot{\lambda} + c_\mu\dot{\gamma} + c_\gamma s_\mu\dot{\chi}\end{aligned}, \tag{5}$$

and

$$\begin{aligned} f_\mu\left(\dot{\theta}_M,\dot{\Lambda},\dot{\lambda},\dot{\chi},\dot{\gamma}\right) = &\left(\left(s_\lambda s_\gamma c_\lambda c_\gamma c_\gamma\right)s_\alpha + \left(c_\lambda s_\chi s_\mu + \left(c_\lambda c_\chi s_\gamma - s_\lambda c_\gamma\right)c_\mu\right)c_\alpha\right)\omega_M\\ &+\left(\left(\left(s_\lambda s_\gamma + c_\lambda c_\chi c_\gamma\right)s_\alpha + \left(c_\lambda s_\chi s_\mu + \left(c_\lambda c_\chi s_\gamma - s_\lambda c_\gamma\right)c_\mu\right)c_\alpha\right)\dot{\Lambda}\right.\\ &+\left(\left(c_\chi s_\mu - s_\chi s_\gamma c_\mu\right)c_\alpha - s_\chi c_\gamma s_\alpha\right)\dot{\lambda} - s_\mu c_\alpha\dot{\gamma} + \left(c_\gamma c_\mu c_\alpha - s_\gamma s_\alpha\right)\dot{\chi}\end{aligned}. \tag{6}$$

Since attitude must be actuated faster than the longitudinal velocity direction, the terms $f_\eta(\cdot)$, $f_\alpha(\cdot)$ and $f_\mu(\cdot)$ can be kept smaller than the first component in the right-hand side of (3). As a further remark, equation (3) becomes undefined for $\alpha = 0$ which is coherent with the fact that the lift becomes zero, and the bank angle μ becomes undefined as soon as the 1-2-1 rotation sequence reduces to single rotation $\mu + \eta$.

The coordinate transformation $\hat{\omega} = R(\eta)\omega$, i.e.

$$\begin{bmatrix}\hat{\omega}_l\\ \hat{\omega}_m\\ \hat{\omega}_n\end{bmatrix} = \begin{bmatrix}1 & 0 & 0\\ 0 & c_\eta & -c_\eta\\ 0 & s_\eta & c_\eta\end{bmatrix}\begin{bmatrix}\omega_l\\ \omega_m\\ \omega_n\end{bmatrix}, \tag{7}$$

simplifies (3) to

$$\begin{bmatrix} \dot{\eta} \\ \dot{\alpha} \\ \dot{\mu} \end{bmatrix} = \begin{bmatrix} 1 & 0 & -c_\alpha / s_\alpha \\ 0 & 1 & 0 \\ 0 & 0 & 1/s_\varepsilon \end{bmatrix} \begin{bmatrix} \widehat{\omega}_l \\ \widehat{\omega}_m \\ \widehat{\omega}_n \end{bmatrix} + \begin{bmatrix} f_\eta\left(\dot{\theta}_M, \dot{\Lambda}, \dot{\lambda}, \dot{\chi}, \dot{\gamma}\right) \\ f_\alpha\left(\dot{\theta}_M, \dot{\Lambda}, \dot{\lambda}, \dot{\chi}, \dot{\gamma}\right) \\ f_\mu\left(\dot{\theta}_M, \dot{\Lambda}, \dot{\lambda}, \dot{\chi}, \dot{\gamma}\right) \end{bmatrix}. \tag{8}$$

C. Equations of dynamics

Assuming that the body frame R_b coincides with the principal inertia frame, Euler dynamic equations read as

$$\begin{bmatrix} \dot{\omega}_l \\ \dot{\omega}_m \\ \dot{\omega}_n \end{bmatrix} = \frac{\left(J_{mn} - J_l\right)}{J_{mn}} \omega_l \begin{bmatrix} 0 \\ \omega_n \\ \omega_m \end{bmatrix} + \begin{bmatrix} \left(M_{a,l} + M_{T,l}\right)/J_l \\ \left(M_{a,m} + M_{T,m}\right)/J_{mn} \\ \left(M_{a,n} + M_{T,n}\right)/J_{mn} \end{bmatrix}, \tag{9}$$

where $M_{a,l-m-n}$ indicates the body components of the aerodynamic torque with respect to the body CoM, and $M_{T,l-m-n}$ denotes the body components of the command torque. J_l denotes the axial component of the diagonal inertia, the other two components are $J_m = J_n = J_{mn}$.

The aerodynamic components $M_{a,l-m-n}$ strictly depend on the capsule aerodynamic properties, and specifically on the CoM offset, indicated with the coordinates x_a^*, y_a^* and z_a^*. Dependence can be proved by writing the equivalent torque coefficients at the center of mass $c_{l,CoM}$, $c_{m,CoM}$ and $c_{n,CoM}$ such that the body coordinates of the aerodynamic torque are

$$\begin{bmatrix} M_{a,l} \\ M_{a,m} \\ M_{a,n} \end{bmatrix} = M_{ref} \begin{bmatrix} c_{l,CoM} \\ c_{m,CoM} \\ c_{n,CoM} \end{bmatrix}, \tag{10}$$

where

$$\begin{aligned} Lc_{l,CoM} &= c_N c_\eta y_a^* - c_N s_\eta z_a^* \\ Lc_{m,CoM} &= c_{m,a} c_\eta - c_N c_\eta x_a^* + c_A z_a^* \\ Lc_{n,CoM} &= -c_{m,a} s_\eta + c_N s_\eta x_a^* - c_A y_a^* \\ M_{ref} &= \frac{1}{2}\rho v^2 LS \end{aligned}. \tag{11}$$

In (11), L and S are, respectively, the scale length and surface of the capsule aerodynamic shape, ρ is the atmospheric density and v the relative velocity magnitude. Further $c_{m,a}$ is the moment coefficient, whereas c_A and c_N are axial and normal force coefficients. They are computed with respect to an aerodynamic frame which is aligned to the principal axis frame R_{as}, and whose origin is displaced from the body CoM by x_a^*, y_a^* and z_a^*. Typically the aerodynamic frame is located one meter behind the top of the capsule end (opposite to the motion direction). For this reason the moment coefficient $c_{m,a}$ is not the main contributor to torque coefficients, but instead c_A and c_N (force coefficients) times their application arms. The coefficients c_N and c_A depend on the total angle of attack α and on the Mach number. Here the equalities $x_a^* = x_a$, $z_a^* = 0$ and $y_a^* = -y_a < 0$ are assumed for simplicity's sake.

The aerodynamic torque with respect to the body CoM is obtained by replacing (10) and (11) in (9), which yields

$$\begin{bmatrix} \dot{\omega}_l \\ \dot{\omega}_m \\ \dot{\omega}_n \end{bmatrix} = \frac{\left(J_{mn} - J_l\right)}{J_{mn}} \omega_l \begin{bmatrix} 0 \\ \omega_n \\ \omega_m \end{bmatrix} + \begin{bmatrix} M_{T,l} / J_l \\ M_{T,m} / J_{mn} \\ M_{T,n} / J_{mn} \end{bmatrix} + \frac{M_{ref}}{L} \begin{bmatrix} -c_N c_\eta y_a / J_l \\ -c_N c_\eta x_a / J_{mn} \\ \left(c_N s_\eta x_a + c_A y_a\right) / J_{mn} \end{bmatrix}. \tag{12}$$

Then, transforming (12) through (7) yields

$$\begin{aligned} &\dot{\hat{\omega}} = \dot{R}(\eta) R^{-1}(\eta) \hat{\omega} + R(\eta) \dot{\omega} = \\ &= \frac{M_{ref}}{L} \begin{bmatrix} -c_N c_\eta y_a / J_l \\ \left(-c_N x_a - c_A s_\eta y_a\right) / J_{mn} \\ c_A c_\eta y_a / J_{mn} \end{bmatrix} + \begin{bmatrix} \hat{u}_l \\ \hat{u}_m \\ \hat{u}_n \end{bmatrix} + \begin{bmatrix} d_j^*\left(\hat{\omega}, \eta, \alpha\right) \\ d_m^*\left(\hat{\omega}, \eta, \alpha\right) \\ d_n^*\left(\hat{\omega}, \eta, \alpha\right) \end{bmatrix}, \end{aligned} \tag{13}$$

where

$$\begin{bmatrix} \hat{u}_l \\ \hat{u}_m \\ \hat{u}_n \end{bmatrix} = R(\eta) \begin{bmatrix} M_{T,l} / J_l \\ M_{T,m} / J_{mn} \\ M_{T,n} / J_{mn} \end{bmatrix}. \tag{14}$$

is the angular acceleration command. In (13), the components $d_{l-m-n}^*\left(\hat{\omega}, \eta, \alpha\right)$ are second order terms encompassing the effects of $\dot{R}(\eta)$ and of the gyro torques.

D. Equilibrium and perturbation equations

Finding the natural equilibrium angles $\underline{\alpha}$ and $\underline{\eta}$ of (8) and (12) ($\underline{\mu} = \mu$ may assume any value) in absence of command torques, i.e. for $\hat{M}_{T,l-m-n} = 0$, is the starting point for rewriting (13) as a perturbation equation. Equilibrium is found for $\hat{\omega}_{l-m-n} = 0$ and for

$$\begin{bmatrix} -c_N c_\eta y_a \\ -c_N x_a - c_A s_\eta y_a \\ c_A c_\eta y_a \end{bmatrix} = 0; \tag{15}$$

and gives rise to the following solutions

$$\begin{aligned} &\underline{\eta} = (2k+1)\pi/2, \; k = ..., -1, 0, 1, ... \\ &c_N\left(\underline{\alpha}\right) x_a = -c_A\left(\underline{\alpha}\right) \sin \underline{\eta}\, y_a = c_A\left(\underline{\alpha}\right) y_a \end{aligned}. \tag{16}$$

Development of the aerodynamic coefficients c_N and c_A in (15) around the equilibrium (16) leads to

$$\begin{aligned} &c_N(\alpha) = \underline{c}_N + \underline{\tau}_{N,1}\left(\alpha - \underline{\alpha}\right) + o_2\left(\left|\alpha - \underline{\alpha}\right|\right) \\ &c_A(\alpha) \cong \underline{c}_A + o_2\left(\left|\alpha - \underline{\alpha}\right|\right) \end{aligned}, \tag{17}$$

having accounted second and higher order terms with $o_2\left(\left|\alpha - \underline{\alpha}\right|\right)$. Equation (17) is employed to derive the linearized version of the attitude kinematics (8) and of the attitude dynamics in (13) for the perturbations

$$\begin{aligned}\Delta\alpha &= \alpha - \underline{\alpha}\\ \Delta\eta &= \eta - \underline{\eta}\end{aligned}. \tag{18}$$

The perturbation equations are written below upon a rearrangement of the state variables so as to show decoupling of the angle of attack from roll and bank angle dynamics:

$$\begin{bmatrix}\dot{\mu}\\ \Delta\dot{\eta}\\ \dot{\widehat{\omega}}_l\\ \dot{\widehat{\omega}}_n\\ \hline \Delta\dot{\alpha}\\ \dot{\widehat{\omega}}_m\end{bmatrix} = \left[\begin{array}{cccc:cc} 0 & 0 & 0 & 1/s_{\underline{\alpha}} & c_{\alpha\mu} & 0\\ 0 & 0 & 1 & -k_\alpha & c_{\alpha\eta} & 0\\ 0 & s_{\underline{\eta}}k_l & 0 & 0 & 0 & 0\\ 0 & -s_{\underline{\eta}}k_n & 0 & 0 & 0 & 0\\ \hdashline 0 & 0 & 0 & 0 & 0 & 1\\ 0 & 0 & 0 & 0 & -k_m & 0\end{array}\right]\begin{bmatrix}\mu\\ \Delta\eta\\ \widehat{\omega}_l\\ \widehat{\omega}_n\\ \hline \Delta\alpha\\ \widehat{\omega}_m\end{bmatrix} + \begin{bmatrix}0\\ 0\\ \widehat{u}_l\\ \widehat{u}_n\\ \hline 0\\ \widehat{u}_m\end{bmatrix} + \begin{bmatrix}f_\mu(\cdot)\\ f_\eta(\cdot)\\ d_l\\ d_n\\ \hline f_\alpha(\cdot)\\ d_m\end{bmatrix} \tag{19}$$

Coefficients in (19) have the following expressions

$$\begin{aligned} &c_{\alpha\mu} = -c_{\underline{\alpha}}/s_{\underline{\alpha}}^2,\ c_{\alpha\eta} = 1/s_{\underline{\alpha}}^2,\ k_\alpha = c_{\underline{\alpha}}/s_{\underline{\alpha}}\\ &k_l = \frac{\underline{c}_N y_a M_{ref}}{J_l L},\ k_n = \frac{\underline{c}_A x_a M_{ref}}{J_{mn} L},\ k_m = \frac{\underline{\tau}_{N,1} x_a M_{ref}}{J_{mn} L}\end{aligned}. \tag{20}$$

Second order terms in (19) and gyroscopic effects are hidden into d_{l-m-n}. Local stability of the equilibrium is obtained from the characteristic polynomial of (19)

$$\begin{aligned}&\lambda^2\left(\lambda^4 + \lambda^2\left(k_m - s_{\underline{\eta}}k_{nl}\right) - s_{\underline{\eta}}k_m k_{nl}\right) = 0\\ &k_{nl} = k_n c_{\underline{\alpha}}/s_{\underline{\alpha}} + k_l\end{aligned}. \tag{21}$$

Eigenvalues of (21) are forced to stay on the imaginary axis by imposing out of (16) the equilibrium

$$\underline{\eta} = -\pi/2,\ s_{\underline{\eta}} = -1. \tag{22}$$

They hold

$$\lambda_{1,2} = \pm j\sqrt{k_m},\ \lambda_{3,4} = 0,\ \lambda_{5,6} = \pm j\sqrt{k_{nl}}. \tag{23}$$

Under condition (22), the equilibrium of total angle of attack derives from (16) and holds

$$c_N(\underline{\alpha})/c_A(\underline{\alpha}) = y_a/x_a > 0. \tag{24}$$

Equation (19) is the simplified dynamic and kinematic equation of the capsule attitude, based on the aerodynamic angles defined above. To better understand the advantage of (19), in contraposition to (3) and (9), the block-diagram of the former one, subdivided between angle of attack, roll and bank angle is shown in Fig 2 and Fig 3. Specifically:

1) The bank angle dynamics is not just second order and forced by the roll torque as in the case of aircrafts, but is fourth order and almost linear ($\Delta\eta$ must be kept small). Roll dynamics plays the role of an internal actuator. The overall dynamics is forced both by roll and yaw torques.
2) The dynamics of the total angle of attack is decoupled from bank angle and roll.

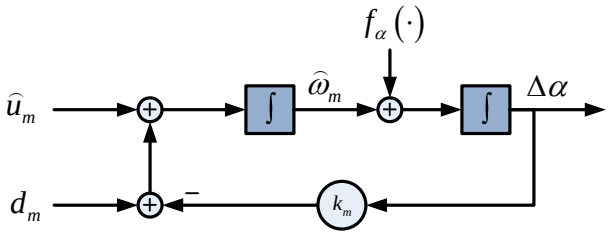

Fig 2. Block-diagram of the perturbed state equation of the angle of attack.

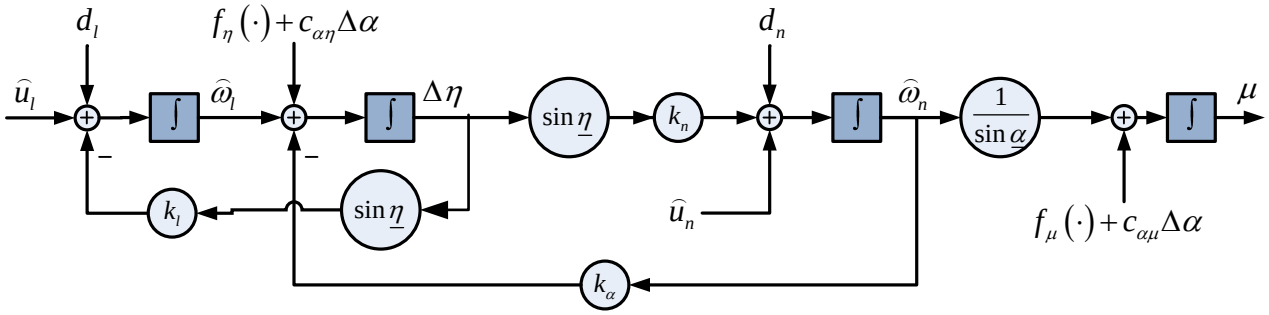

Fig 3. Block-diagram of the state equations of the bank angle and roll perturbations.

E. Roll and bank angle decoupling

A further decomposition aims to open the loop in Fig 3 between roll and bank angle, having the feedback gain k_α in (20). By opening the loop, the bank angle dynamics would become in series with the roll dynamics, whose output $\Delta\eta$ should be kept close to zero (the natural equilibrium) by the roll control. As a result, the bank angle dynamics would be only driven by the transformed command $\widehat{u}_n$. The decoupling mechanism, to be outline below, is such to generate a coupling with the rate $\dot{\alpha}$ of the total angle of attack (entering the functions $g_x(\cdot)$, $x=\alpha,\eta,\mu$ to be defined below). Also the latter rate should be kept close to zero (the natural equilibrium) by the angle-of-attack control.

The decoupling mechanism passes through the second derivative of (19), which after some manipulation becomes

$$\begin{bmatrix}\Delta\ddot{\eta}\\ \ddot{\mu}\\ \Delta\ddot{\alpha}\end{bmatrix}=\begin{bmatrix}-a_\eta & 0 & -a_{\eta\alpha}\\ 0 & a_\mu & a_{\mu\alpha}\\ 0 & 0 & -k_m\end{bmatrix}\begin{bmatrix}\Delta\eta\\ \mu\\ \Delta\alpha\end{bmatrix}+\begin{bmatrix}b_{\eta\alpha}\\ -b_{\mu\alpha}\\ 0\end{bmatrix}\Delta\dot{\alpha}+\begin{bmatrix}1 & -c_{\underline{\alpha}}/s_{\underline{\alpha}} & 0\\ 0 & 1/s_{\underline{\alpha}} & 0\\ 0 & 0 & 1\end{bmatrix}\begin{bmatrix}\widehat{u}_l\\ \widehat{u}_n\\ \widehat{u}_m\end{bmatrix}+\begin{bmatrix}d_\eta\\ d_\mu\\ d_\alpha\end{bmatrix}. \tag{25}$$

Coefficients in (25) are as follows

$$\begin{aligned}&a_\eta=k_l+k_n c_{\underline{\alpha}}/s_{\underline{\alpha}},\ a_{\eta\alpha}=2c_{\underline{\alpha}}/s_{\underline{\alpha}}^3,\ a_\mu=k_n/s_{\underline{\alpha}}\\ &a_{\mu\alpha}=\frac{1}{s_{\underline{\alpha}}}\left(1+2\left(\frac{c_{\underline{\alpha}}}{s_{\underline{\alpha}}}\right)^2\right)\\ &b_{\eta\alpha}=\frac{1}{s_{\underline{\alpha}}^2},\ b_{\mu\alpha}=\frac{c_{\underline{\alpha}}}{s_{\underline{\alpha}}^2}\end{aligned}\quad . \tag{26}$$

Input variables (disturbance terms) are found to be

$$
\begin{aligned}
&d_\eta = d_l - d_n c_{\underline{\alpha}} / s_{\underline{\alpha}} + g_\eta(\cdot),\ d_\mu = d_n / s_{\underline{\alpha}} + g_\mu(\cdot)\\
&d_\alpha = d_l + g_\alpha(\cdot)\\
&g_\mu(\cdot) = \dot{f}_\mu + \frac{\dot{\underline{\alpha}} c_{\underline{\alpha}}}{s_{\underline{\alpha}}}\left(f_\mu(\cdot) - \mu\right)\\
&g_\eta(\cdot) = \dot{f}_\eta - \frac{\dot{\underline{\alpha}}}{s_{\underline{\alpha}}} f_\mu(\cdot) + \frac{\dot{\underline{\alpha}}\dot{\mu}}{s_{\underline{\alpha}}},\ g_\alpha(\cdot) = \dot{f}_\alpha(\cdot)
\end{aligned}
\qquad . \tag{27}
$$

One may observe that $\Delta\alpha$ is decoupled from roll and bank angle, but affects them. Moreover the bank angle command $\hat{u}_n$ enters also the roll equation, that is the first one in (25).

It is now viable to define a decoupled command vector $u = \begin{bmatrix} u_\eta & u_\mu & u_\alpha \end{bmatrix}^T$, such that each component drives a single aerodynamic angle. The following dispatching equation, obtained by inverting the input matrix in (25), provides the new command components (in angular acceleration units)

$$
\begin{bmatrix} \hat{u}_l \\ \hat{u}_n \\ \hat{u}_m \end{bmatrix} = \begin{bmatrix} 1 & c_{\underline{\alpha}} & 0 \\ 0 & s_{\underline{\alpha}} & 0 \\ 0 & 0 & 1 \end{bmatrix} \begin{bmatrix} u_\eta \\ u_\mu \\ u_\alpha \end{bmatrix}. \tag{28}
$$

The attitude control can now be designed using u_η, u_μ and u_α as commands. Specifically u_η and u_α are computed for damping the angular rates $\hat{\omega}_l$ and $\hat{\omega}_m$, respectively, and u_μ is computed for driving the bank angle based on the requested profile of the longitudinal and lateral CoM control.

III. Attitude Control

A. Reference generator of the bank angle control

Only the bank angle needs a reference generator to provide the reference profiles to be tracked. Angle of attack and roll must be only stabilized around their natural (unknown) equilibriums, which corresponds to a zero reference for $\Delta\eta$ and $\Delta\alpha$, as well as for their rates and accelerations.

Following (25), the bank angle control is designed assuming a simplified second order dynamics (the cascade of two integrators). It is arranged following EMC into (i) a reference generator (the open-loop control, Fig 5) providing the reference bank angle $\underline{\mu}$ together with the first and second derivatives $\dot{\underline{\mu}}$ and $\underline{u}_\mu = \ddot{\underline{\mu}}$, (ii) a control law, combination of open-loop command, state feedback and disturbance rejection, (iii) the discrete time embedded model (combination of controllable and disturbance dynamics, Fig 6) and (iv) the noise estimator (Fig 6) providing in real-time the noise vectors updating the unknown disturbance dynamics. The bank angle control becomes the actuator of the translational control in Canuto et al. [2]. The latter provides the required bank angle profile μ_{des}, which is decomposed into the reference bank angle cosine $\cos\underline{\mu}_p$ and the time instants t_{br} of the bank reversal maneuvers. The reference bank angle $\underline{\mu}_p$ computed by the path-planning algorithm $\underline{\mu}_p$ must be corrected by the variation Δu_{dr}.

In the course of a bank reversal maneuver a jump of the reference bank angle from $\underline{\mu}_0$ to $\underline{\mu}_1$ is performed, with the following constraints.

1) The cosine of the bank angle reaches its nominal value at the end of the maneuver

$$\cos\underline{\mu}_1 = \cos\underline{\mu}_0 . \tag{29}$$

2) The sign of the bank angle sine toggles

$$\operatorname{sign}\left(\sin\underline{\mu}_1\right) = -\operatorname{sign}\left(\sin\underline{\mu}_0\right). \tag{30}$$

3) The derivative of the cosine of the bank angle remains constant

$$\frac{d}{dt}\cos\underline{\mu}_1 = \frac{d}{dt}\cos\underline{\mu}_0 . \tag{31}$$

4) The maximum value $u_{\mu,\max}$ of the reference bank angle acceleration $\underline{u}_\mu$ remains bounded.

The maneuver is the result of a bang-bang control capable of moving $\underline{\mu}_0$ to $\underline{\mu}_1$ and matching the constraints (29), (30) and (31). The approach aims to attenuate distortions on the profile of u_{dr}. Assume that the maneuver starting time $t = 0$ is reached. The maneuver starts by using $\underline{\mu}_0 = \underline{\mu}(0)$ and $\dot{\underline{\mu}}_0 = \dot{\underline{\mu}}(0)$ to build the bank angle profile. The bang-bang control is split in two intervals $0 \le t \le T_{sw}$ and $T_{sw} \le t \le T_{br}$ where $\underline{u}_\mu$ is forced to the maximum value and changes sign as in Fig 4.

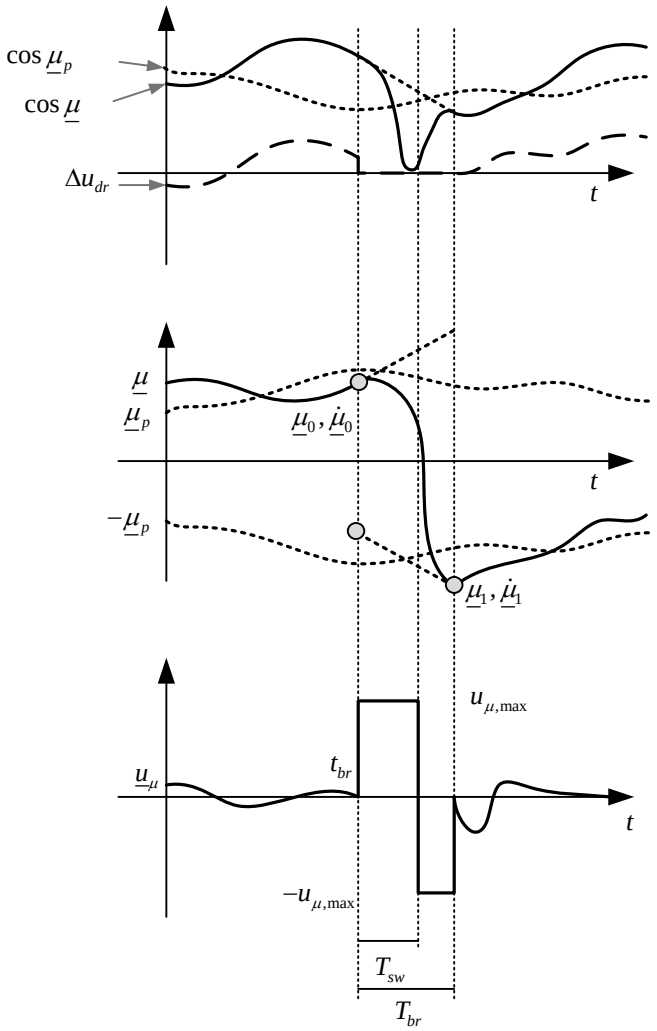

Fig 4. Time profile of typical signals during a bank reversal maneuver.

Expressions of the bank angle and of the rate during the maneuver allows to compute the maneuver duration T_{br} and the switching time T_{sw} , by imposing the above constraints. The bank angle rate at the maneuver end

$$\dot{\underline{\mu}}_1\left(T_{br}\right) = \dot{\underline{\mu}}_0 - u_{\mu,\max}T_{sw} + u_{\mu,\max}\left(T_{br} - T_{sw}\right) = -\dot{\underline{\mu}}_0 , \tag{32}$$

allows to find the switching time in terms of T_{br} as follows

$$T_{sw} = \frac{\dot{\underline{\mu}}_0 + (T_{br}/2)u_{\mu,\max}}{u_{\mu,\max}} . \tag{33}$$

The angular position at T_{br} holds

$$\underline{\mu}_1(t+T_{br}) = \underline{\mu}_0 - \dot{\underline{\mu}}_0 T_{sw} - \frac{1}{2}u_{\mu,\max}T_{sw}^2 + \left(-\dot{\underline{\mu}}_0 - u_{\mu,\max}T_{sw}\right)\left(T_{br}-T_{sw}\right) + \frac{1}{2}u_{\mu,\max}\left(T_{br}-T_{sw}\right)^2 . \tag{34}$$

By replacing (33) into (34), the expression of T_{br} is found

$$T_{br} = 2\frac{\sqrt{2\left(\underline{\mu}_0 u_{\mu,\max} + \dot{\underline{\mu}}_0^2\right)} - 2\,\dot{\underline{\mu}}_0}{u_{\mu,\max}} . \tag{35}$$

Outside bank reversal maneuvers (not reported here) the bank angle must track the requested variation of the lift vertical component coming from the translational control. The attitude control computes, at each step, the reference bank angle μ_{des} from

$$\mu_{des} = \cos^{-1}\left(\cos\underline{\mu}_p + \Delta u_{dr}\right) . \tag{36}$$

The reference generator in Fig 5 uses μ_{des} to build its second derivative $\underline{u}_\mu$ using a dynamic feedback (see Canuto et al.[8]). In this manner, not only $\underline{u}_\mu$ is obtained, but also $\underline{\mu}$ and $\dot{\underline{\mu}}$, with the condition that $\underline{\mu}$ tends to track μ_{des}. The block-diagram is shown in Fig 5. Blocks with the symbol Σ denote discrete-time integrators having Z-transform $(z-1)^{-1}$. The state q is part of the output dynamics feedback. The gains a_0, k_1, k_0 are computed to provide the resulting closed-loop system with appropriate eigenvalues.

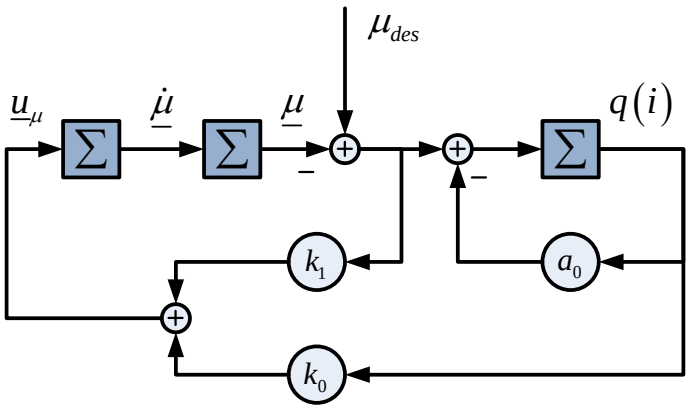

Fig 5. Bank angle open-loop control

B. Attitude control law

The attitude control law receives (i) the reference state and command from the reference generator (only for the bank angle), (ii) controllable and disturbance state variables $\hat{x}_{d,l-m-n}$ from the attitude embedded model, to be described below. Based on such data, it computes one-step-ahead the command vector u (in angular acceleration units) to be converted by (28) and (14) into the torque components $M_{T,l-m-n}$. Command torques are then dispatched to the reaction control system.

The embedded model is based on the simplified attitude dynamics in Fig 2 and Fig 3, and in (19), but is extended to include the disturbance dynamics as shown in Fig 6. Since $\Delta\alpha$ and $\Delta\eta$ are not controlled and are unknown, they are not included in the embedded model. In fact, angle of attack and roll are just stabilized by a rate feedback around their (unknown) natural equilibriums. By the way, roll and angle of attack could not be controlled around given reference values, because of the limited authority of the reaction control system.

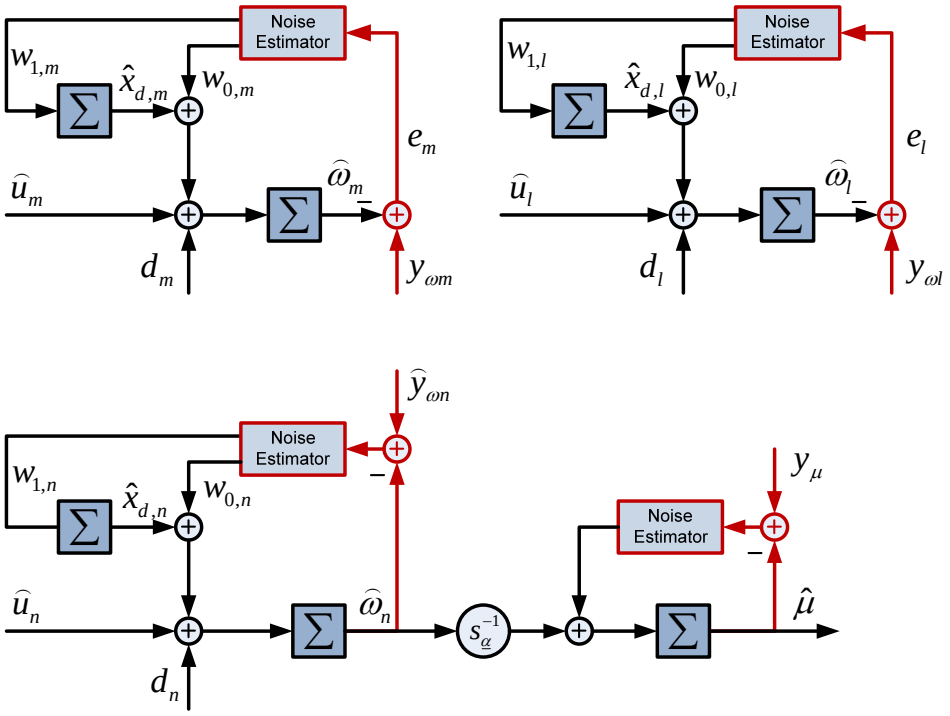

Fig 6. The attitude embedded model

The principles of the attitude control law are as follows.

1) The known disturbances d_l, d_m and d_n in (19) are computed and cancelled by their respective collocated commands, which is equivalent to a nonlinear dynamic inversion.
2) The residuals (due to parametric errors and neglected terms) are estimated using the embedded model and the navigation data, and are compensated by collocated commands.
3) A feedback is implemented from $\hat{\omega}_l$ and $\hat{\omega}_m$ to $\hat{u}_l$ and $\hat{u}_m$, respectively, in Fig 2 and Fig 3, to damp $\Delta\eta$ and $\Delta\alpha$ around their natural equilibriums. The feedback gain $k_{0,l}$ and $k_{0,m}$ are computed from (20) to fix the damping ratio of the resulting second order dynamics.
4) A state feedback is implemented from $\dot{\mu}$ and μ to u_μ in Fig 3, in order to stabilize bank angle and rate around their reference values. Feedback gains $k_{0,n}$ and $k_{1,n}$ are computed by pole placement, to fix the desired natural frequency and damping factor.

The resulting control laws expressed in continuous time (they are actually implemented in discrete-time like the embedded model) are

$$\begin{bmatrix} \hat{u}_l \\ \hat{u}_m \\ \hat{u}_n \end{bmatrix}(t) = \begin{bmatrix} 0 \\ 0 \\ \underline{u}_\mu \end{bmatrix}(t) + \begin{bmatrix} -k_{0,l}\hat{\omega}_l \\ -k_{0,m}\hat{\omega}_m \\ k_{0,n}\left(\underline{\dot{\mu}} - \mu\right) \end{bmatrix}(t) + \begin{bmatrix} 0 \\ 0 \\ k_{1,n}\left(\underline{\mu} - \mu\right) \end{bmatrix}(t) - \begin{bmatrix} x_{d,l} + d_\eta \\ x_{d,m} + d_m \\ x_{d,n} + d_n \end{bmatrix}(t). \tag{37}$$

The thrust forces of the thruster assembly are computed through an appropriate dispatching algorithm, depending on the assembly geometry. Finally, in the case that pulsed thrusters are employed, thrusts are converted into duty cycles. The block-diagram of the overall attitude control system is shown in Fig 7.

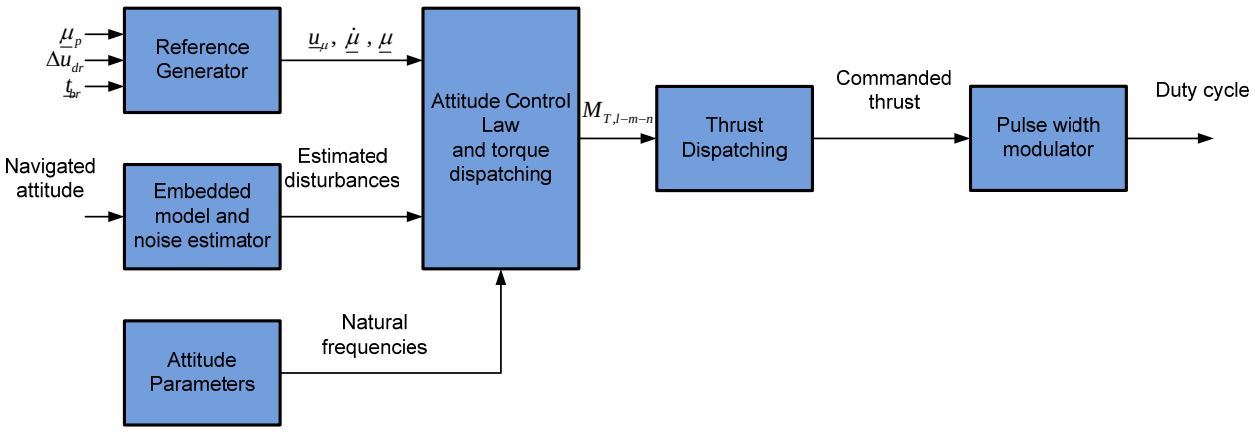

Fig 7. Block diagram of the overall attitude control.

IV. Simulated results

The simulated results of a single the Monte Carlo run out are presented and discussed. Nominal parameters and dispersions of are summarized in Table 1. The sampling frequency of the attitude control was designed to be 10 Hz. Although a 5 Hz frequency (2.5 Hz being the Nyquist frequency) would have been preferred, being more suitable to off-the-shelf pulsed thrusters, analysis and simulated runs pointed out that a 5 Hz-sampled control law was incapable of damping aerodynamic angles during the whole entry phase. A critical phase occurs when dynamic pressure reaches the maximum value, and the aerodynamic-angle natural frequencies settle around 1 Hz, just 2.5 times smaller than Nyquist frequency.

Table 1. Parameters and initial state of the Monte Carlo simulations

Var.	Units	Value	Disp. 3σ	Var.	Units	Value	Disp. 3σ .
$r(t_{ein})$	[m]	3516200	5 000	c_A	[–]		10 %
$\Lambda(t_{ein})$	[deg]	0	10 000	c_N	[–]		10 %
$\lambda(t_{ein})$	[deg]	0	10 000	$u_{dr}(0)$	[–]	-0.5	-
$v(t_{ein})$	[m/s]	5560	20	$u_{T,\max}$	[N]	160	10 %
$\gamma(t_{ein})$	[deg]	-13.4	0,05	J_{xx}	[kg/m^2]	2400	5 %
$\chi(t_{ein})$	[deg]	90	0,05	J_{vv}	[kg/m^2]	2000	5 %
m	[kg]	2200	1 %	J_{zz}	[kg/m^2]	1400	5 %
Δx_{CoM}	[m]	0.1	0.005	$J_{xy-xz-yz}$	[kg/m^2]	0	10
ρ	[kg/m^3]	EMCD	EMCD				

EMCD =European Mars Climate Database

Fig 8 shows the evolution of the aerodynamic angles α and η as they track their Mach-varying equilibriums. One may observe that oscillations are rather negligible showing a correct damping of (37) along the whole flight regime. Fig 9, left, and Fig 10, right, illustrate the bank angle profile (reference and navigated), showing that the navigated angles closely tracks the reference. The tracking error of the bank angle in Fig 9, right, shows some significant perturbations. They coincide with bank reversal maneuvers; but, even at those occurrences, tracking error remains well below 2 degrees. The commanded torque in Fig 10, left, remains bounded as it closely follows the reference bank angle acceleration computed by the attitude reference generator. The torque which is a sequence of doublets is the second derivative of the bank angle profile.

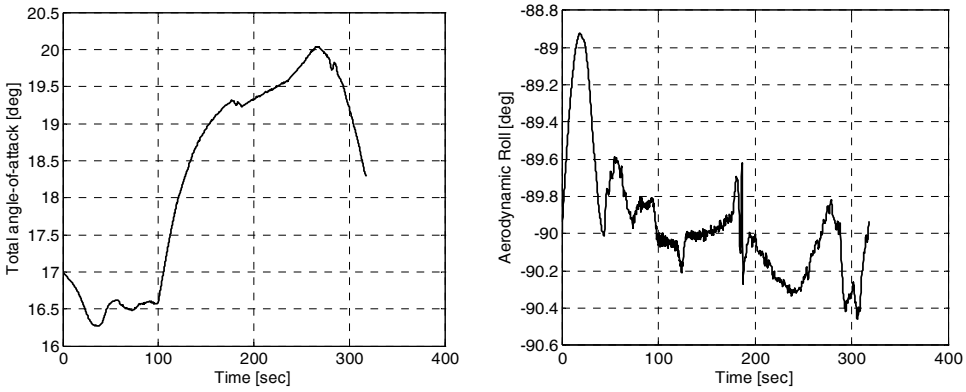

Fig 8. Time evolution of total angle of attack (left) and aerodynamic roll (right).

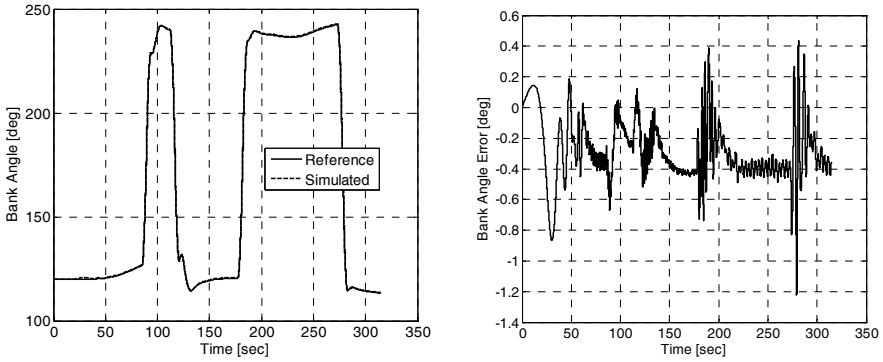

Fig 9. Bank angle (left) and tracking error (right).

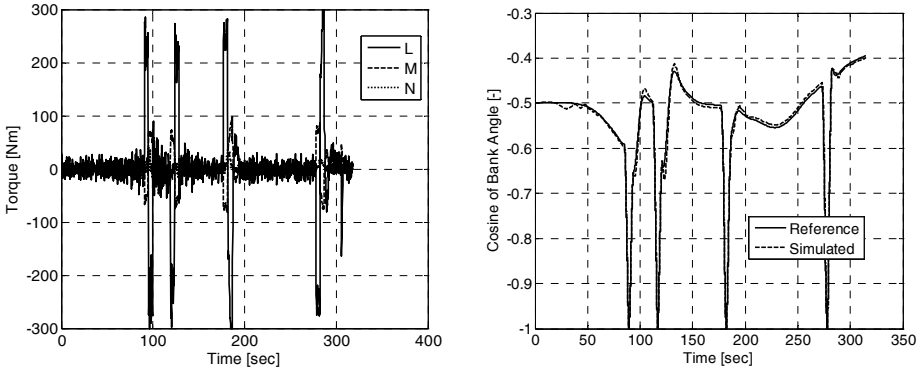

Fig 10. Commanded torque (left) and cosine of the bank angle (right).

V. Conclusion

The attitude control system of a planetary landing capsule during atmospheric entry has been proved it can be designed around the triplet of 'axisymmetric' aerodynamic angles (total angle of attack, roll and bank angle) instead of using either Euler angles or quaternions. A model-based control algorithm has been proposed which combines open loop commands (output of a reference generator), active disturbance cancellation and state feedback, in agreement with the Embedded Model Control methodology.

Theoretical analysis (only provided without proofs) and simulated results concur to the fact that a tight and effective control of aerodynamic angles, especially of the bank angle around the required trajectory, can be achieved only if roll and angle of attack are well damped. This fact entails that control algorithms should pay attention not to

excite their dynamics. Technological considerations, as those concerning control sampling frequency, mass consumption and minimum impulse bit of the reaction control system are relevant and should be better investigated.

Acknowledgments

One of the authors is grateful to Thales Alenia Space Italia for the financial support.

References

1 Wolf, A. , Tooley, J., Ploen, S., Ivanov, M., Acikmese, B., and Gromov, K., "Performance Trades for Mars Pinpoint Landing," *2006 IEEE Aerospace Conference*, IEEE, 2006, pp. 1-16, doi: 10.1109/AERO.2006.1655793.

2 Canuto, E., Ospina, J., and Buonocore, M., "Model-based guidance and control for atmospheric guided entry," *AIAA Guidance, Navigation, and Control Conference*, 13-16 August, 2012, Minneapolis, MA.

3 Brugarolas, P. B., San Martin, A.M., and Wong, E. C., "Entry Attitude Controller for the Mars Science Laboratory," *2007 IEEE Aerospace Conference*, March 2007, pp. 1-6, doi: 10.1109/AERO.2007.352824.

4 Kron, A., and de Lafontaine J., "Control of Mars guided entry (Part II): Robust nonlinear dynamics inversion," *Automatic Control in Aerospace*, Vol. 17, Part I, Elsevier, 2007, pp. 581-586, doi: 10.3182/20070625-5-FR-2916.00099.

5 Canuto, E., "Embedded Model Control: outline of the theory," *ISA transactions*, Vol. 46, No. 3, June 2007, pp. 363-77, doi: 10.1016/j.isatra.2007.01.006.

6 Canuto, E., "Drag-free and attitude control for the GOCE satellite," *Automatica*, Vol. 44, No. 7, July 2008, pp. 1766-1780, doi: 10.1016/j.automatica.2007.11.023.

7 Canuto, E., Molano, A., and Massotti, L. "Drag-free control of the GOCE satellite: noise and observer design, " *IEEE Trans. Control Systems Technology*, March 2010, Vol. 18, No. 2, pp. 501-509, doi: 10.1109/TCST.2009.2020169.

8 Canuto, E., Acuna Bravo, W., A. Molano-Jimenez, A., and Perez-Montenegro, C., "Embedded Model Control calls for disturbance modelling and rejection," *ISA Transactions*, Vol. 51, No. 5, 2012, pp. 584-595, doi: 10.1016/j.isatra.2012.04.002.

9 Gallais, P., *Atmospheric Re-Entry Vehicle Mechanics*, Springer, 2007.